Simulation study of desalination performance for two large-scale air gap membrane distillation modules

H. Chang*, Y.-H. Chou, C.-D. Ho, C.-L. Chang, H.-J. Chen

Energy and Opto-Electronic Materials Research Center, Department of Chemical and Materials Engineering, Tamkang University, New Taipei, Taiwan
Tel. +886 (2) 2623 2094; Fax: +886 (2) 2620 9887; email: nhchang@mail.tku.edu.tw

ABSTRACT

Being capable of utilizing low-grade thermal energy, membrane distillation (MD) has evolved as a promising technology for desalination. This paper reports the simulation study of two large-scale MD modules reported in the literature, a spiral wound type and a flat plate type. A mathematical model, which considers the heat and mass transfer mechanisms for all the composing layers of the module, is used. For both modules, the heat and mass transfer resistance and the performance enhancement by modifying design parameters and operating conditions are analyzed. The significant directions and quantitative potential of improvement are identified. Compared to the bases cases, the flux enhancement from modifying module parameters can be as high as about 10% for the spiral wound module and about 100% for the flat plate module. The flux enhancement from modifying operation conditions can be as high as about 50% for both modules.

Keywords: Air gap membrane distillation; Membrane distillation; Desalination; Modeling

1. Introduction

Membrane distillation (MD) is a thermally driven separation process, in which only vapor molecules are transported through porous hydrophobic membranes. The driving force is the vapor pressure difference between the hot liquid feed side and the cold permeate side of the membrane. MD systems can be classified into four configurations according to the nature of the cold side of the membrane, i.e. direct contact MD (DCMD), air gap MD (AGMD), sweeping gas MD, and vacuum MD (VMD). The principles, applications, and developments of MD have been comprehensively reviewed by several researchers [1–3].

Compared to other desalination technologies, the MD desalination system is highly competitive mainly due to its low operating cost by using the low-grade heat, such as the solar thermal energy. Many papers have been published on this application, including those on the desalination processes [4,5] and on the modeling and experimental studies of the performances, operation and control of the MD modules as well as the solar powered desalination systems [6–15]. Several experimental studies of solar driven MD desalination systems, where the thermal energy for MD is supplied by solar collectors, have demonstrated the feasibility with large-scale devices [10–15].

Developments in configuration designs for MD-related desalination processes have recently

---

*Corresponding author.

evolved. Multi-stage MD concept for solar desalination application has been proposed and different multi-stage designs have been evaluated for high-efficiency and cost-effective stand-alone seawater desalination system [16]. It has also been claimed feasible to integrate VMD, to treat highly concentrated water, with conventional reverse osmosis desalination for system performance enhancement [17]. Guijt et al. [18] described the novel Memstill® module, which is a hollow fiber AGMD module with heat integration design between the counter-current flow hot and cold fluids. Compared to multi stage flash (MSF), MD, and RO desalination technologies, the energy consumption of the Memstill® technology can be about 50% lower.

Because it is the heart of the desalination system, many researchers have focused on the performance enhancement of MD modules. Two significant studies were conducted on laboratory-scale modules. Cath et al. [19] proposed a vacuum enhanced DCMD configuration using flat-sheet composite membrane with very thin active layers and operated under very high Reynolds number flow operation. The membrane water flux can be increased dramatically to 85 kg/(m²h), which is 2–30 times higher than literature data. Song et al. [20] reported the experimental results of hollow fiber DCMD with cross-flow configuration to enhance mass transport coefficients and using a membrane coated with an additional porous highly hydrophobic layer to prevent the wetting of membrane. The study showed that stable and high flux of 55 kg/(m²h) can be obtained for long time operation. For practical applications, particularly for solar desalination, large-scale modules have been developed and reported recently. Winter et al. [15] reported experimental results for full-scale spiral wound modules of 5–14 m² membrane area each module, including the effects of feed flow rate, temperature levels, salinity, and membrane area. Guillén-Burrieza et al. [10] reported pilot operation data for a solar desalination plant using full-scale flat plate-and-frame AGMD modules of 2.8 m² membrane area of each module. The MD module performance varied with the daily solar irradiation and is difficult to discuss independently. A systematic analysis for large-scale modules is essential and a comprehensive and verified mathematical model can be an effective tool for the study.

In this paper, a theoretical model considering the heat and mass transfer mechanisms based on our previous work [8] is used for the systematical study of two large-scale AGMD modules—a spiral wound type and a flat plate type. The heat and mass transfer resistance analysis as well as the parameter analysis are conducted. The objective is to shed light on the significant improvements for practical applications.

2. Mathematical model

The AGMD model adopted is the same as that reported in our previous work [8] and the model has been verified with experimental results from laboratory-scale flat plate modules [6,9] as well as large-scale spiral wound module [21]. For the former, experimental studies covered both the operation conditions, including the flow rate and inlet temperature of hot and cold fluids, and the module parameters, including the thickness of hot fluid channel, cold fluid channel, and air gap. The differences between the simulation and experimental results are less than 10%. For the latter, the effects of hot fluid flow rate and temperature were compared and shown in Fig. 1. For higher fluid flow rates, the results are fairly close. However, the simulation results are higher than the experimental data for low flow rate conditions. One possible cause is the heat loss from the module to the environment. When the fluid flow rate is lower, the effect of heat loss on the hot fluid temperature will be greater.

The model is one dimensional and the interface fluxes are determined by heat and mass transfer correlations from literature. The porous membrane is filled with water vapor and air. The fluids in the channels are plug flow without pressure drop.

The mass and energy fluxes for all layers, including the hot fluid, membrane, air gap, condensing liquid, metal plate, and cold fluid, are illustrated in Fig. 2. The model equations are summarized in Table 1. In the model, the mass transfer flux is determined by considering the mass transfer resistances in the membrane and air gap, because the resistances of the hot fluid side, cold fluid side, and condensing liquid are insignificant [8]. With its small flow rate, the condensate film is very thin and the heat transfer resistance is neglected. The heat transfer resistances of all other layers are taken into account.

The heat and mass transfer coefficients needed in the model are calculated using the equations listed in Table 2. For the hot fluid and cold fluid, because L/D_e is greater than $Re/20$, the entrance effect can be neglected [22]. The heat transfer coefficients are estimated using correlations for flat plate [23]. For spiral wound module analysis, because the channel heights are very small compared to the module dimensions, the same correlation for flat plate module is used. For the membrane and metal plate, the thermal conductivities and thicknesses of these materials are used for calculating the heat transfer coefficients. In Eq. (24), the thermal conductivity of membrane (K_{mem}) is computed as the volume average of the vapor conductivity and the solid polymer membrane conductivity. Other thermally related properties, which are assumed
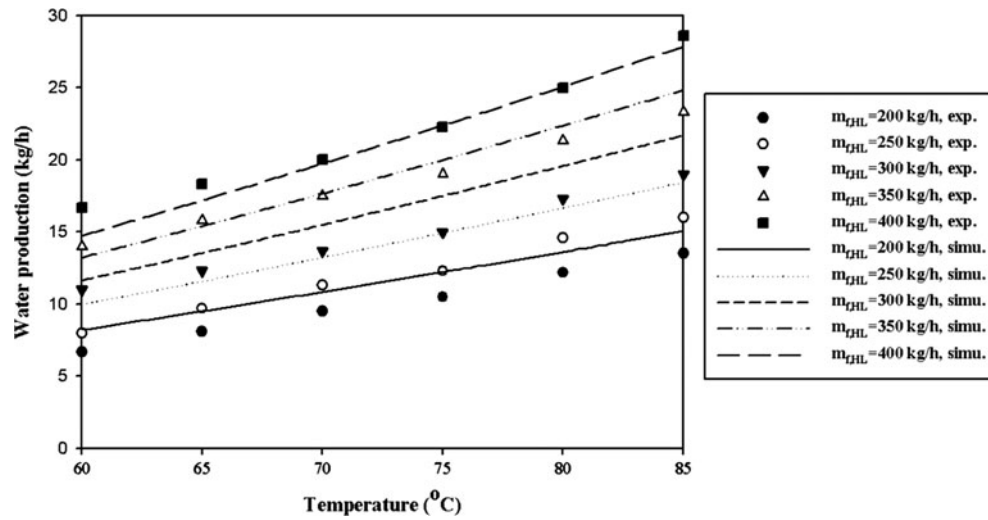
Fig. 1. Comparison of model simulation and experimental data from Ref. [21].
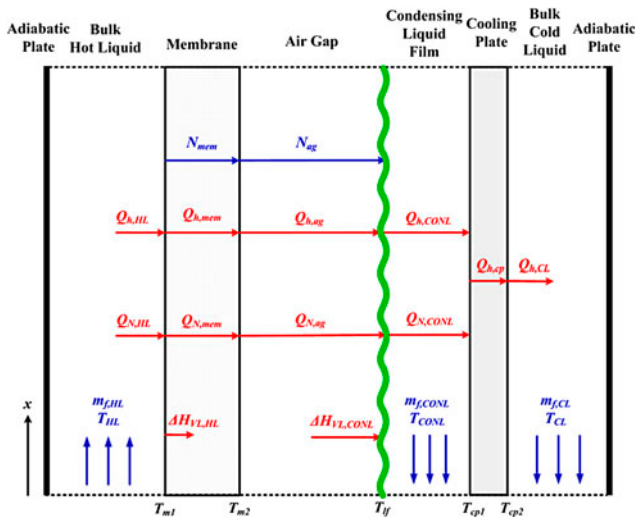

Fig. 2. Heat and mass transfers in AGMD module.

constant, include the thermal conductivities, heat capacities, and heat of vaporization.

For the mass transfer in the porous membrane, Knudsen diffusion and molecular diffusion are taken into account via the resistance-in-series approach as shown in Eq. (27). For the air gap with a thickness of only several mm, the mass transfer coefficient is estimated from the diffusivity of water vapor in air by Eq. (28). The Knudsen diffusivity is calculated using Eqs. (6.5–14) in [24]. The molecular diffusivities are estimated by the empirical equation of Fuller et al. [25].

The model equations are solved using implicit Euler and Newton methods.

3. Results and discussion

For practical application of the solar powered MD desalination technology, several large-scale or pilot processes have been operated and reported [10–15]. The modules applied are mainly AGMD type and in spiral wound or flat plate shapes, as shown in Fig. 3 (a) [15] and Fig. 3(b), respectively. For investigating the potential of improvement for large-scale AGMD modules employed for practical applications, two modules with the specifications, which are mostly based on the information from the literature [10,15], listed in Table 3 are studied in this paper. The table also includes the base operating conditions. Both modules are operated in the laminar region, but the Re number of the spiral wound module is smaller, the reason should be that the pressure drop is higher due to the much longer flow channel feature.

The approaches for this study include: (1) analysis of the heat and mass transfer resistances for each layer of the module to identify the significant layers, and (2) sensitivity analysis of device parameters and operating conditions for their effects on the module performance, i.e. the water flux, in order to identify the important parameters and conditions. All these analyses and discussion are based on the module parameters and operation conditions listed in Table 3.

3.1. Analysis of heat and mass transfer resistances

The resistance analysis is conducted by sensitivity analysis by adjusting the heat and mass transfer coefficients of each layer, via the use of a multiplier of 0.1 or 10 in the mathematical model. The effects on water

Table 1
Model equations for SAF–AGMD

Mass balances		Heat fluxes	
$\frac{dm_{f,HL}}{dx} = -N_{mem}Mw_{water}W$	(1)	$Q_{h,HL} = h_{HL}(T_{HL} - T_{m1})$	(12)
$\frac{dm_{f,CONL}}{dx} = -N_{ag}Mw_{water}W$	(2)	$Q_{N,HL} = N_{mem}C^L_{p,HL}(T_{HL} - T_{m1})$	(13)
$N_{mem} = N_{ag}$	(3)	$\Delta H_{VL,HL} = N_{mem}\Delta H_{vap,m1}$	(14)
Energy balances		$Q_{h,mem} = h_{mem}(T_{m1} - T_{m2})$	(15)
$\frac{m_{f,HL}}{M_{HL}}\frac{\partial T_{HL}}{\partial x} = -\frac{W}{M_{HL}C^L_{p,HL}}(Q_{h,HL} + Q_{N,HL})$	(4)	$Q_{N,mem} = N_{mem}C^V_{p,mem}(T_{m1} - T_{m2})$	(16)
$\frac{m_{f,CL}}{M_{CL}}\frac{\partial T_{CL}}{\partial x} = -\frac{W}{M_{CL}C^L_{p,CL}}Q_{h,CL}$	(5)	$Q_{h,ag2} = h_{ag2}(T_{m2} - T_{mp1})$	(17)
$Q_{h,HL} + Q_{N,HL} - \Delta H_{VL,HL} = Q_{h,mem} + Q_{N,mem}$	(6)	$Q_{N,ag2} = N_{ag2}C^V_{p,ag2}(T_{m2} - T_{mp1})$	(18)
$Q_{h,mem} + Q_{N,mem} = Q_{h,ag} + Q_{N,ag}$	(7)	$\Delta H_{VL,CONL} = N_{ag2}\Delta H_{vap,mp1}$	(19)
$Q_{h,ag} + Q_{N,ag} + \Delta H_{VL,CONL} = Q_{h,mp}$	(8)	$Q_{h,mp} = h_{hp}(T_{mp1} - T_{mp2})$	(20)
$Q_{h,mp} = Q_{h,CL}$	(9)	$Q_{h,CL} = h_{CL}(T_{mp2} - T_{CL})$	(21)
Mass fluxes			
$N_{mem} = \frac{k_{mem}}{RT_{mem}}(P_{m1,water} - P_{m2,water})$	(10)		
$N_{ag} = \frac{k_{ag2}P_{sys}}{RT_{ag2}P_{ag2,lm}}(P_{m2,water} - P_{LF,water})$	(11)		

Table 2
Estimation of transfer coefficients

Heat transfer coefficient of fluid		
For hot fluid (h_{HL}) and cold fluid (h_{CL})	$Nu = 1.86(RePr\frac{D_e}{L})^{0.33}$ $Re < 2,100$	(22)
	$Nu = 0.023Re^{0.8}Pr^n$ $2,500 < Re < 1.25\times10^5, 0.6 < Pr < 100$	(23)
	$n = 0.4$ for cold fluid, $n = 0.3$ for hot fluid	
Heat transfer coefficient of membrane (h_{mem})	$h_{mem} = \frac{K_{mem}}{\delta_{mem}}$	(24)
Heat transfer coefficient of air gap (h_{ag})	$h_{ag} = \frac{K_{ag}}{\delta_{ag}}$	(25)
Heat transfer coefficient of metal plate (h_{mp})	$h_{mp} = \frac{K_{mp}}{\delta_{mp}}$	(26)
Mass transfer coefficient of membrane (k_{mem})	$k_{mem} = \frac{\varepsilon}{\tau}\left[\frac{1}{1/D_k + y_{air,lm}/D_m}\right]\frac{1}{\delta_{mem}}$	(27)
Mass transfer coefficient of air gap (k_{ag})	$k_{ag} = \frac{D_m}{\delta_{ag}}$	(28)

fluxes are then examined. The identification of significant transfer coefficients can suggest the directions for improving the module performance. The heat transfer resistances of four layers are examined, including hot fluid, membrane, air gap, and cold fluid. The top and bottom plates of the module are assumed well insulated. The condensing film is difficult to modify and the metal plate has very high thermal conductivity, hence these two parts are excluded in the analysis. As for the mass transfer resistances, only the membrane layer and air gap layer need to be considered. For these two layers, the analysis includes modifying only the heat transfer coefficient, only the mass transfer coefficient, and simultaneously the heat and mass transfer coefficients.

For the spiral wound module, the results shown in Fig. 3(a)–(c) indicate:

- For both hot and cold fluids, increasing the heat transfer resistance can significantly reduce the flux, but reducing the resistance can only slightly increase the flux as shown in Fig. 4(a).
- Also shown in Fig. 4(a), for both membrane and air gap layers, the increase of the heat transfer coefficient in these layers will decrease the temperature difference between the two sides of the membrane or air gap layer and reduce the vapor pressure difference, which is the driving force for the mass transfer. The effect of air gap layer is greater than the membrane layer.
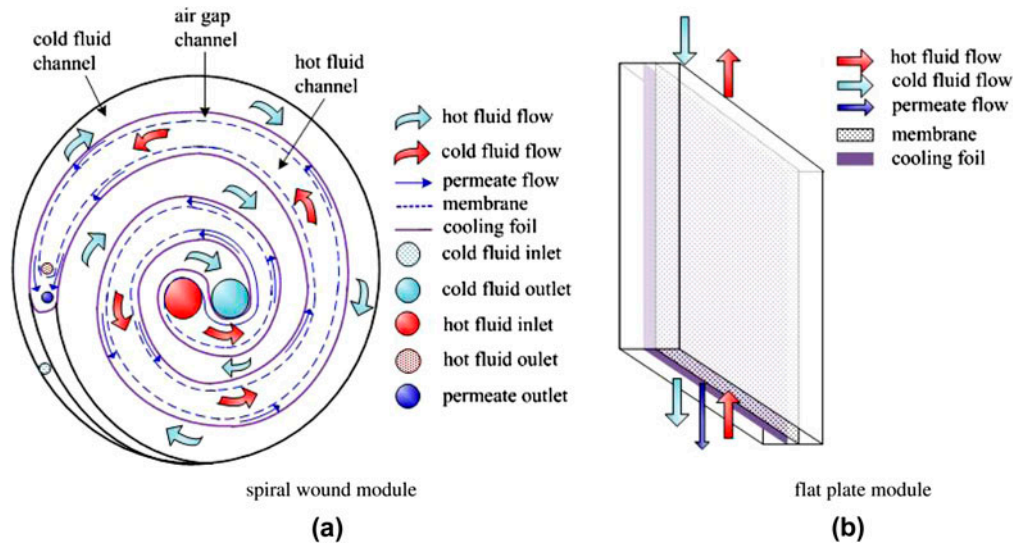
Fig. 3. Spiral wound and flat plate modules.

Table 3
Specifications of large-scale modules

Parameters	Spiral wound	Flat plate
Membrane area (m^2)	10	2.8 (for 20 flat-sheet membranes)
Membrane width (m)	0.7	0.36
Membrane length (m)	14.29	0.39
Membrane material	PTFE + PP	PTFE + PP
Membrane thickness (μm)	30/140	30/170
Membrane pore diameter (μm)	0.1	0.2
Membrane porosity	0.72	0.8
Height of hot fluid channel (mm)	0.77	1
Height of cold fluid channel (mm)	0.77	1
Thickness of air gap (mm)	0.43	1
Hot and cold fluids flow configuration	Counter-current	Counter-current
Operating pressure (atm)	1	1
Hot fluid temperature (K)	348	348
Cold fluid temperature (K)	293	293
Hot fluid flow rate (kg/h)	300	375
Re of hot fluid	300	1,459
Cold fluid flow rate (kg/h)	300	375
Re of cold fluid	339	665

- For both membrane and air gap layers, the increase of the mass transfer coefficient can enhance the flux as shown from Fig. 4(b). The effect on flux is greater in the direction of reducing resistance.

- When the heat and mass transfer resistances are simultaneously changed by the same degree for the membrane and air gap layers, the effects are opposite and the combined effect depends on the relative extents. As illustrated in Fig. 4(c), the combinatory effects are different for the two layers. For the membrane layer, the effect of mass transfer coefficient is greater than that of the heat transfer coefficient. Hence, the combined effect is the same as that from the mass transfer coefficient. However, for the air gap layer, the combined effect is that the flux is reduced by either direction of modifications.

For the flat plate module, the results shown in Figs. 4(d)–(f) indicate:

- For the hot and cold fluids, as shown in Fig. 4(d), decreasing the heat transfer coefficient causes the reduction of the flux. The effects are significant in both directions for hot fluid, but only in the direction of decreasing the coefficient for cold fluid.
- In Fig. 4(d), the effects of varying heat transfer coefficient are small for both membrane and air gap layers.
- The effects of varying mass transfer coefficient are significant in both directions for air gap layer, but only in the direction of decreasing the coefficient for the membrane layer as indicated in Fig. 4(e).
- When comparing Figs. 4(e) and (f), it can be found that the combined effects of heat and mass transfer coefficients are the same as those of the mass transfer coefficient. It is because the effects of heat transfer coefficient are small.
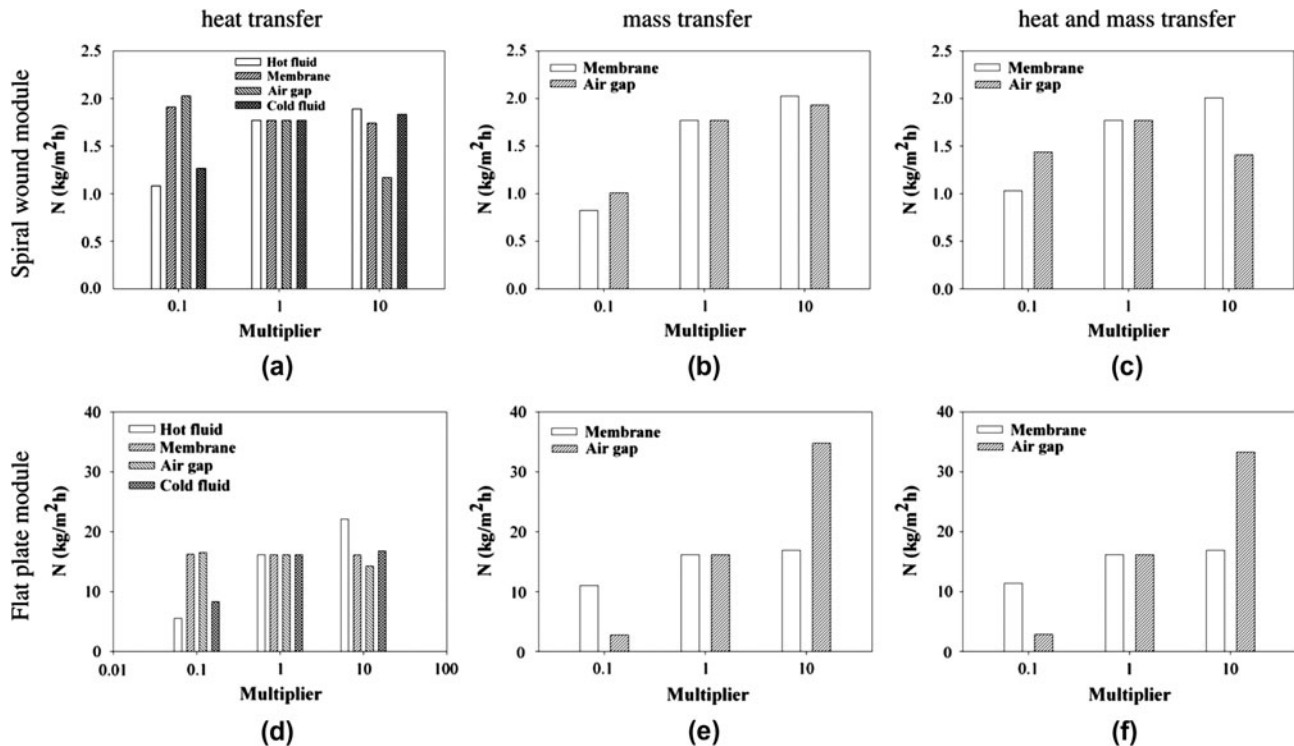
Fig. 4. Analysis of heat and mass transfer resistances.

In summary, although the flux levels of the two types of modules are different, the trends of influences are similar, except on the effects of mass transfer coefficient and combined heat and mass transfer coefficients on the air gap layer. The reason lies on the big difference in the layer thickness, 0.43 mm for the spiral wound module and 1 mm for the flat plate module. For the spiral wound module, the gap is much thinner and its contribution to the overall resistance is not significant, hence little improvement of the module performance can be obtained. However, for the flat plate module, the improvement of heat and/or mass transfer of the air gap layer can lead to significant enhancement for module performance. When considering the effective measures for module performance improvement from the base cases of these two modules, one should focus on the membrane layer and the air gap layer for the spiral wound module and the flat plate module, respectively.

3.2. Effects of device parameters and operating conditions

The study of performance improvement is accomplished by individually varying each device parameter and operating condition for the two large-scale modules. The device parameters examined include the channel height of hot fluid and cold fluid, the air gap thickness and all variable membrane characteristics, i. e. the thicknesses of porous and supporting layers, the pore diameter, the membrane porosity, and the membrane length to width ratio. The operating conditions include the flow rates of hot and cold fluids (Re number), the temperatures of hot and cold fluids, and the operating pressure of air gap.

Some of the parameters or conditions pose only minor effects on the water flux. For those which pose relatively significant effects, the results are given in Fig. 5 and Fig. 6 for the spiral wound module and flat plate module, respectively.

For the device parameters, the significant ones are different for the two modules. For the spiral wound module, the porous layer thickness and membrane porosity are important. On the other hand, for the flat plate module, the important parameters are the hot fluid channel height, air gap thickness, and membrane length. The effects on water flux by varying each parameter are shown in Figs. 4(a) and (b) and Figs. 5 (a)–(c). Compared to the bases cases, the flux enhancement from modifying module parameters can be as high as about 10% for the spiral wound module and about 100% for the flat plate module.

On operating conditions, the hot fluid temperature, cold fluid temperature, and Re numbers of both fluids are important ones for both modules. However, the
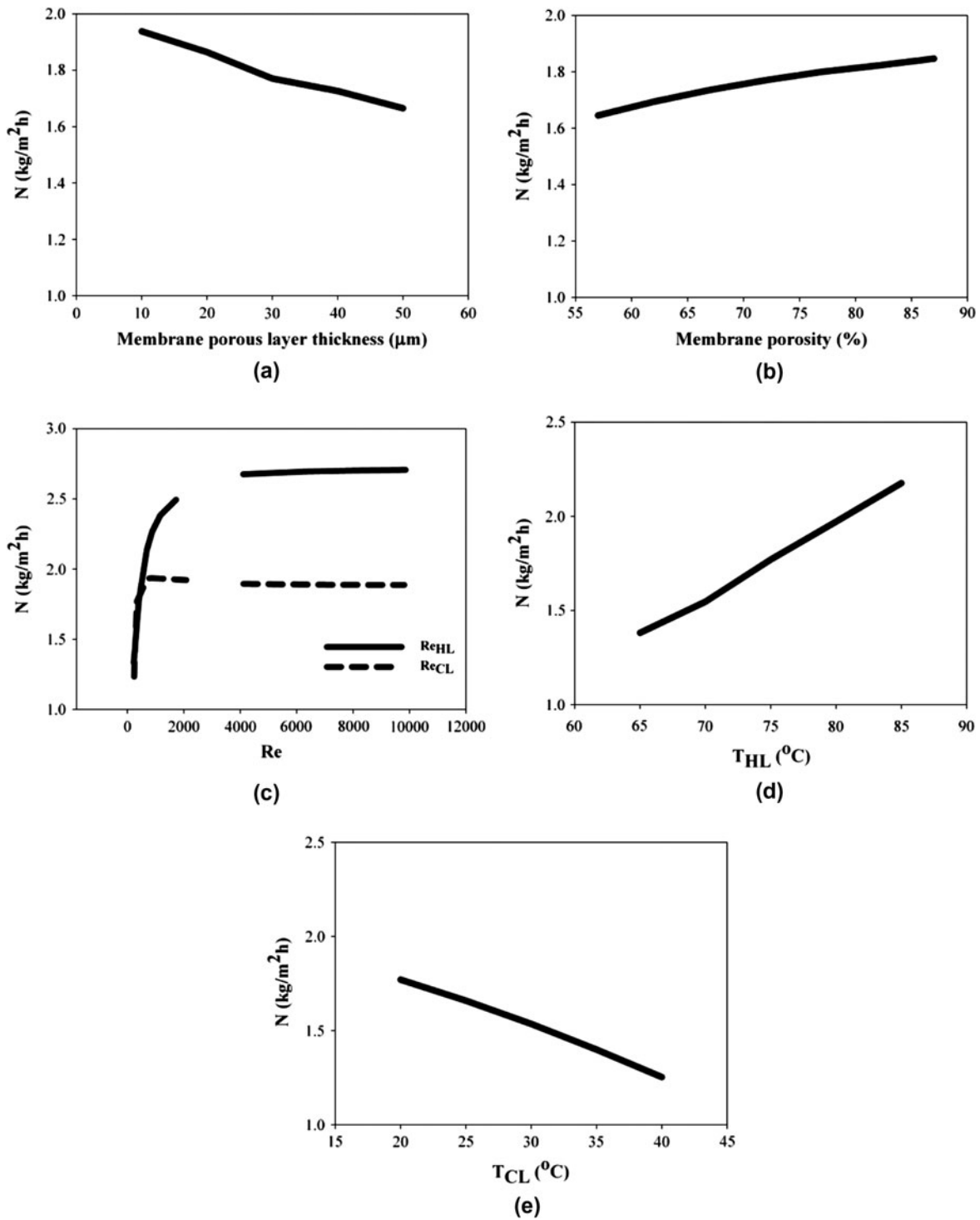
Fig. 5. Significant variables for spiral wound module.

air gap operating pressure is significant only to the flat plate module. The extents of water flux variation when varying each condition variable are shown in Figs. 4(c)–(e) and Figs. 5(d)–(g). The hot fluid temperature provides greater effect on water flux. The positive effect of increasing Re number is noteworthy only for laminar region, if the flow is in turbulent range, the effect is limited. Note that in Figs. 5(c) and
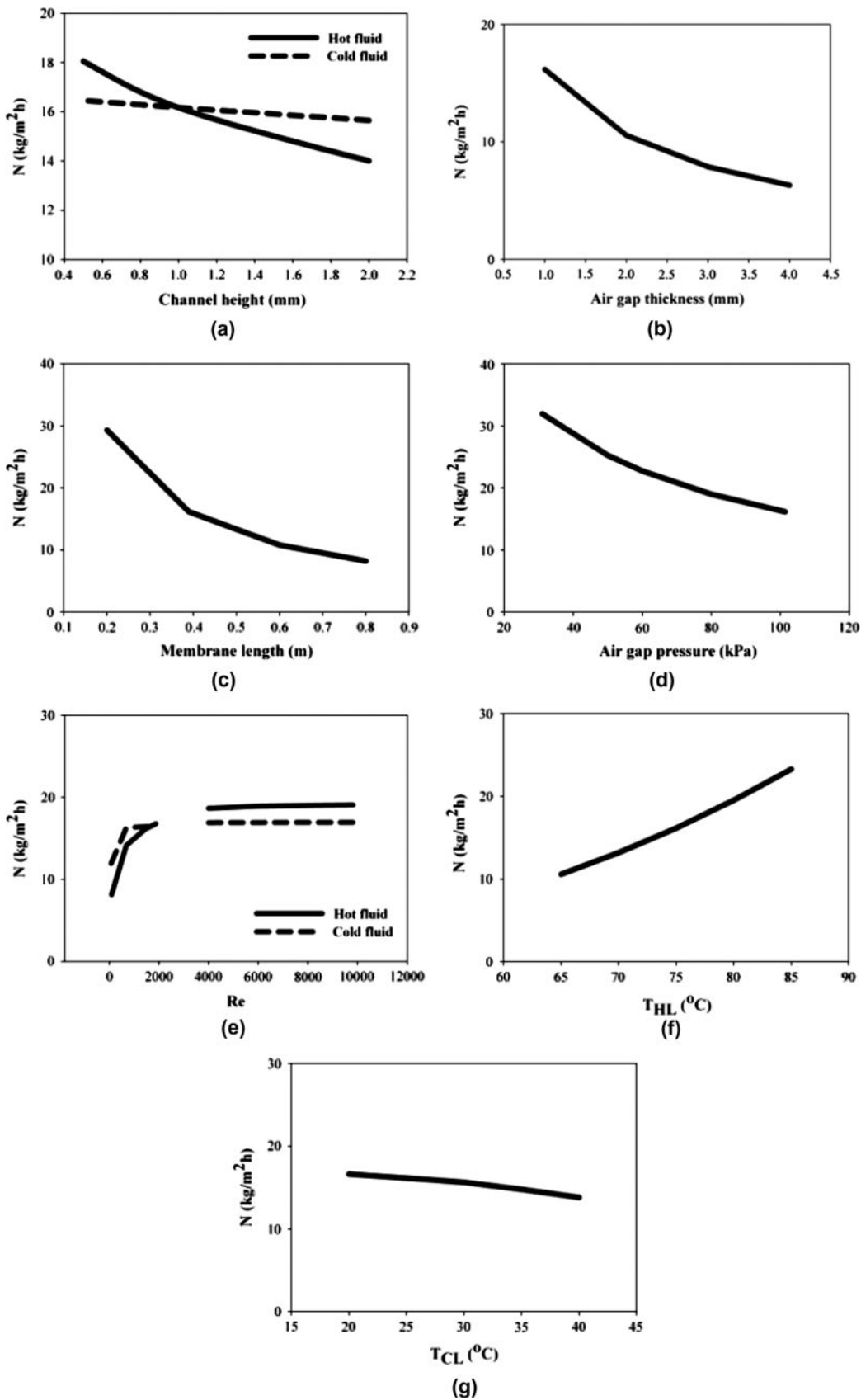
Fig. 6. Significant variables for flat plate module.

6(e), the transitional flow region is not analyzed. Compared to the bases cases, the flux enhancement from modifying operation conditions can be as high as about 50% for both modules.

4. Conclusions

For the air gap MD, we have accomplished the examination of the performance characteristics and performance enhancement potentials for two large-scale modules for practical applications. Based on the module parameters and the base case operating conditions specified in this study, comparisons on the spiral wound module and flat plate modules have been made. The resistance analysis reveals that the flat plate module provides much higher potential for improvement than the spiral wound module. For the device parameters, the significant ones are different for the two modules. For the spiral wound module, porous layer thickness and membrane porosity are important. On the other hand, for the flat plate module, the important parameters are hot fluid channel height, air gap thickness, and membrane length. Compared to the bases cases, the flux enhancement from modifying module parameters can be as high as about 10% for the spiral wound module and about 100% for the flat plate module. On operating conditions, the hot fluid temperature, cold fluid temperature, and Re numbers of both fluids are important ones for both modules. Compared to the bases cases, the flux enhancement from modifying operation conditions can be as high as about 50% for both modules.

A final remark on the two modules can be made. Compared to the flat plate module, the spiral wound module operates with only about 1/10 of the membrane flux. That can be explained from the mathematical model. The significantly longer module length of the spiral wound module results in much lower heat transfer coefficients in the fluid sides using the correlations listed in Table 2. That further consequences the very different results of the two modules in the resistance analysis and parameter study.

Symbols

$AGMD$	—	air gap membrane distillation
C_p	—	heat capacity (J/kg K)
D_e	—	hydraulic diameter (m)
D_m	—	molecular diffusivity (m^2/s)
D_k	—	Knudsen diffusivity (m^2/s)
$DCMD$	—	direct contact membrane distillation

h	—	heat transfer coefficient (W/m^2 K)
k	—	mass transfer coefficient (m/s)
K	—	Thermal conductivity (W/m K)
L	—	Length of the module (m)
M	—	Mass of the hot or cold fluid in the module (kg)
M_w	—	molecular weight of water (kg/kmol)
MD	—	membrane distillation
m_f	—	mass flow rate (kg/s)
N	—	mole flux of water (kmol/m^2 s)
Nu	—	Nusselt number
P	—	pressure (Pa)
Pr	—	Prandtl number
Q_h	—	heat transfer rate by convection or conduction (J/s)
Q_N	—	heat transfer rate by the temperature change of the water flux (J/s)
R	—	gas constant (Pa m^3/kmol K)
Re	—	Reynolds number
T	—	temperature (K)
$\bar{T}$	—	average temperature (K)
W	—	Width of the module (m)
y	—	molar fraction

Greek letters

ΔH_{VL}	—	enthalpy of vapor–liquid phase change (J/m^2 s)
ΔH_{vap}	—	heat of vaporization (J/kmol)
δ	—	thickness (m)
ε	—	porosity of the membrane
τ	—	tortuosity of the membrane

Superscripts

L	—	liquid
V	—	vapor

Subscripts

Air	—	air
ag	—	air gap
CL	—	cold liquid
CONL	—	condensing liquid
HL	—	hot liquid
LF	—	air gap two-condensing liquid interface
lm	—	logarithmic mean
m1	—	hot fluid–membrane interface
m2	—	membrane–air gap interface
mem	—	membrane
mp	—	metal plate
mp1	—	air gap–metal plate interface
mp2	—	metal plate–cold fluid interface
sys	—	system
water	—	water

Acknowledgment

The authors thank the funding (NSC-100-2621-M-032-004) from the National Science Council of Taiwan.

References

[1] D.R. Lloyd, K.W. Lawson, Membrane distillation, J. Membr. Sci. 124 (1997) 1–25.

[2] A.M. Alklaibi, N. Lior, Membrane-distillation desalination: Status and potential, Desalination 171 (2004) 111–131.

[3] M.S. El-Bourawi, Z. Ding, R. Ma, M. Khayet, A framework for better understanding membrane distillation separation process, J. Membr. Sci. 285 (2006) 4–29.

[4] S. Al Obaidan, E. Curcio, G. Di Profio, E. Drioli, The role of membrane distillation/crystallization technologies in the integrated membrane system for seawater desalination, Desalin. Water Treat. 10 (2009) 210–219.

[5] K. Murase, Y. Yamagishi, K. Tano, Development of a hybrid solar distillator of a basin type distillator and a membrane distillatory, Desalin. Water Treat. 9 (2009) 96–104.

[6] H. Chang, C.-L. Chang, C.-D. Ho, C.-C. Li, P.-H. Wang, Experimental and simulation study of an air gap membrane distillation module with solar absorption function for desalination, Desalin. Water Treat. 25 (2011) 251–258.

[7] H. Chang, J.-S. Liau, C.-D. Ho, W.-H. Wang, Simulation of membrane distillation modules for desalination by developing user's model on Aspen Plus platform, Desalination 249 (2009) 380–387.

[8] H. Chang, G.-B. Wang, Y.-H. Chen, C.-C. Li, C.-L. Chang, Modeling and optimization of a solar driven membrane distillation desalination system, Renewable Energy 35 (2010) 2714–2722.

[9] H. Chang, S.-G. Lyu, C.-M. Tsai, Y.-H. Chen, T.-W. Cheng, Y.-H. Chou, Experimental and simulation study of a solar thermal driven membrane distillation desalination process, Desalination 286 (2012) 400–411.

[10] E. Guillén-Burrieza, J. Blanco, G. Zaragoza, D.C. Alarcón, P. Palenzuela, M. Ibarra, W. Gernjak, Experimental analysis of an air gap membrane distillation solar desalination pilot system, J. Membr. Sci. 379 (2011) 386–396.

[11] J.B. Gálvez, L. García-Rodríguez, I. Martín-Mateos, Seawater desalination by an innovative solar-powered membrane distillation system: The MEDESOL project, Desalination 246 (2009) 567–576.

[12] F. Banat, N. Jwaied, M. Rommel, J. Koschikowski, M. Wieghaus, Performance evaluation of the large SMADES autonomous desalination solar-driven membrane distillation plant in Aqaba, Jordan, Desalination 217 (2007) 17–28.

[13] F. Banat, N. Jwaied, M. Rommel, J. Koschikowski, M. Wieghaus, Desalination by a compact SMADES autonomous solar-powered membrane distillation unit, Desalination 217 (2007) 29–37.

[14] J. Van Medevoort, A. Jansen, J.H. Hanemaaijer, C. Dotremont, B. Nelemnas, E. Van Sonsbeek, Memstill: Seawater desalination a solution to water scarcity, in: BMG-NMG Membrane Symposium, Belgian Membrane Group, Antwerp, Belgium, November 26, 2008.

[15] D. Winter, J. Koschikowski, M. Wieghaus, Desalination using membrane distillation: Experimental studies on full scale spiral wound modules, J. Membr. Sci. 375 (2011) 104–112.

[16] J.C. Vega-Beltrán, L. García-Rodríguez, I. Martín-Mateos, J. Blanco-Gálvez, Solar membrane distillation: Theoretical assessment of multi-stage concept, Desalin. Water Treat. 18 (2010) 133–138.

[17] J.-P. Mericq, S. Laborie, C. Cabassud, Vacuum membrane distillation for an integrated seawater desalination process, Desalin. Water Treat. 9 (2009) 287–296.

[18] G.W. Meindersma, C.M. Guijt, A.B. de Haan, Desalination and water recycling by air gap membrane distillation, Desalination 187 (2006) 291–301.

[19] T.Y. Cath, B. Dean Adams, A.E. Childress, Experimental study of desalination using direct contact membrane distillation: A new approach to flux enhancement, J. Membr. Sci. 228 (2004) 5–16.

[20] L. Song, B. Li, K.K. Sirkar, J.L. Gilron, Direct contact membrane distillation-based desalination: Novel membranes, devices, larger-scale studies, and a model, Indust. Eng. Chem. Res. 46 (2007) 2307–2323.

[21] J. Koshchikowski, M. Wieghaus, M. Rommel, Solar thermal-driven desalination plants based on membrane distillation, Desalination 156 (2003) 295–304.

[22] W. Kays, M.E. Crawford, Convective Heat and Mass Transfer, Second ed., McGraw-Hill, New York, NY, 1980.

[23] J.P. Holman, Heat Transfer, McGraw-Hill, New York, NY, 1989.

[24] E.L. Cussler, Diffusion: Mass Transfer in Fluid Systems, second ed., Cambridge University Press, New York, NY, 1997.

[25] E.N. Fuller, P.D. Schettler, J.C. Giddings, A new method for prediction of binary gas-phase diffusion coefficients, Indust. Eng. Chem. Res. 58 (1966) 18–27.